Spectrochimica Acta Part A: Molecular and Biomolecular Spectroscopy 248 (2021) 119189

Contents lists available at ScienceDirect

Spectrochimica Acta Part A: Molecular and Biomolecular Spectroscopy

journal homepage: www.elsevier.com/locate/saa

Short Communication

Biomolecular alterations in acute traumatic brain injury (TBI) using Fourier transform infrared (FTIR) imaging spectroscopy

Fazle Rakib [a], Khalid Al-Saad [a], Tariq Ahmed [b], Ehsan Ullah [c], George E. Barreto [d,e], Ghulam Md Ashraf [f,g,*], Mohamed H.M. Ali [b,*]

[a] Department of Chemistry and Earth Sciences, Qatar University, Doha, Qatar
[b] Qatar Biomedical Research Institute, Hamad Bin Khalifa University, Doha, Qatar
[c] Qatar Computing Research Institute, Hamad Bin Khalifa University, Doha, Qatar
[d] Department of Biological Sciences, University of Limerick, Limerick, Ireland
[e] Health Research Institute, University of Limerick, Limerick, Limerick, Ireland
[f] King Fahd Medical Research Center, King Abdulaziz University, Jeddah, Saudi Arabia
[g] Department of Medical Laboratory Technology, Faculty of Applied Medical Sciences, King Abdulaziz University, Jeddah, Saudi Arabia

HIGHLIGHTS

- Traumatic injury results in brain metabolic dysfunction.
- We assessed brain biochemistry using Fourier transform infrared spectroscopy.
- We observed a reduction in lipid acyl chains with an increase in methyl (–CH_3) and unsaturated lipids olefin = CH.
- Brain injury induces a reduction in total lipid and total protein in different brain areas.

GRAPHICAL ABSTRACT

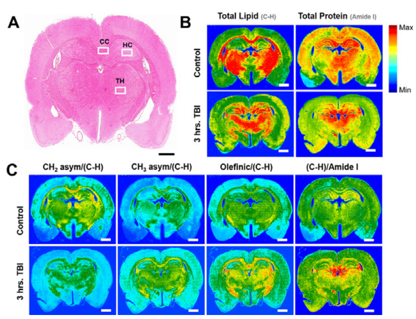

ARTICLE INFO

Article history:
Received 31 October 2019
Received in revised form 27 October 2020
Accepted 1 November 2020
Available online 13 November 2020

Keywords:
Infrared imaging
Acute brain, injury
Biochemical mapping
Hippocampus
Corpus callosum
Thalamus
FTIR
Traumatic brain injury

ABSTRACT

Acute injury is one of the substantial stage post-traumatic brain injury (TBI) occurring at the moment of impact. Decreased metabolism, unregulated cerebral blood flow and direct tissue damage are triggered by acute injury. Understating the biochemical alterations associated with acute TBI is critical for brain plasticity and recovery. The objective of this study was to investigate the biochemical and molecular changes in hippocampus, corpus callosum and thalamus brain regions post-acute TBI in rats. Fourier Transform Infrared (FTIR) imaging spectroscopy were used to collect chemical images from control and 3 hrs post-TBI (Marmarou model was used for the TBI induction) rat brains and adjacent sections were treated by hematoxylin and eosin (H&E) staining to correlate with the disruption in tissue morphology and injured brain biochemistry. Our results revealed that the total lipid and total protein content decreased significantly in the hippocampus, corpus callosum and thalamus after brain injury. Reduction in lipid acyl chains (–CH_2) associated with an increase in methyl (–CH_3) and unsaturated lipids olefin = CH concentrations is observed. Furthermore, there is a decrease in the lipid order (disorder), which leads to an increase in acyl chain fluidity in injured rats. The results suggest acute TBI damages brain tissues mechanically rather than chemical alterations. This will help in assessing successful therapeutic strategy in order to mitigate tissue damage in acute TBI period.

* Corresponding authors at: King Fahd Medical Research Center, King Abdulaziz University, Jeddah, Saudi Arabia (G.M. Ashraf). Qatar Biomedical Research Institute, Hamad Bin Khalifa University, Doha, Qatar (M.H.M. Ali).

E-mail addresses: gashraf@kau.edu.sa (G. Md Ashraf), mohamali@hbku.edu.qa (M.H.M. Ali).

https://doi.org/10.1016/j.saa.2020.119189
1386-1425/© 2020 The Authors. Published by Elsevier B.V.

1. Introduction

Traumatic Brain Injury is defined as damage to the brain from an external force, affecting over 10 million people globally, and is believed to surpass many diseases as the leading cause of mortality in the year 2020 [1,2]. The uneven topography of the inner surface of certain skull regions are factors that result in heightened vulnerability to impact forces (shear, tensile, and compression forces) for certain brain regions [3,4]. TBI has maximum impact on axons and blood vessels, tissue tears, and intracerebral hematomas [3,5]. Early traumatic injury results in metabolic, mitochondrial dysfunction, cellular and molecular alterations causing ultimate cell death (apoptotic and necrotic), neurotransmitter and excitatory amino acid release, inflammation and tissue damage [6–8]. Interstitial levels of excitatory amino acids, such as glutamate, are increased which leads to depolarization, cellular swelling, calcium influx, and neuronal cell death. Cerebral glucose utilization is considerably increased in response to released ions and excitatory amino acids which is called hyper glycolysis [9,10].

Cognitive, emotional, behavioral, and sensorimotor disturbances are the principal clinical manifestations of TBI throughout the early post injury period [8]. Certain regions have a heightened vulnerability to this injury including the corpus callosum, the rostral brainstem, focal cortical contusion and diffuse subcortical (such as hippocampus and thalamus), the deeper midline structures including the basal ganglia and the sub frontal white matter [5,8,11,12]. Brain injuries are diagnosed by using computerized tomography (CT) and/or Magnetic Resonance imaging (MRI). CT and MRI are designed to detect areas of bleeding or after a period of time remnant of blood called (hemosiderin) [13]. Large quantity or red blood cells must hemorrhage from blood vessel or blood vessels to be detected by CT or MRI. Unless of blood vessel or multiple vessels are torn creating relatively large bleed. These technologies failed to demonstrate and find the presence of multiple, widespread and microscopic axonal injuries that could have devastating neuropsychological deficits.

Rapid advances in imaging technologies have pushed forward innovative spectroscopic modalities such as Fourier transform infrared spectroscopy (FTIR) to the forefront of direct in situ investigation of brain biochemistry [14]. In contrast to the standard histological staining methods, FTIR is the "state-of-the-art" biodiagnostic and bio-imaging technology for fast diagnosis in medicine and biological studies [15–17]. As the molecule absorbs the electromagnetic radiation, it produces a band in the infrared (IR) spectrum due to the vibration of atoms at specific wavenumber [18]. The IR spectral vibrational wavenumber provide information about bio-molecules, and produce unique biochemical and biophysical fingerprint for proteins, lipids, cholesterols, phospholipids, carbohydrates, and nucleic acids. FTIR spectroscopy is a simple, sensitive, accurate, highly reproducible, non-destructive (with respect to sample preparation), and rapid, diagnostic technique. FTIR imaging spectroscopy has also been used to analyze the pathological changes associated with breast cancer [16,19,20], stroke [15,17,21], Parkinson's disease [22–24] and other neurodegenerative diseases [18,25,26].

FTIR technology is relatively straightforward and rapid. There is no requirement of prior treatment of brain samples with dyes, or reagents, in order to characterize the different brain structures, and the technique, in addition, is non-destructive, which allows the sample to be analyzed with additional techniques [15,17,19]. Hence, FTIR can be a fast, reproducible technique, in order to characterize the biochemical make-up of various brain regions [17], to provide a good platform for investigating brain alterations at the molecular-level, such as in the cases of neurological disorders [15,17,27–29]. The aim of this study is to elucidate the biomolecular and chemical information that underlie changes with brain injury in critical brain regions post-acute stage of TBI and their possible effect on the brain function.

2. Results

Fourier transform infrared imaging spectroscopy to identify the chemical alterations in the experimental animals post-acute TBI.

FTIR spectroscopy monitors the vibrational modes of functional groups within biomolecules and enables a correlation between chemical information and histological structures [32–34]. Shifts in peak positions, changes in bandwidths, intensities, and band area values in the IR spectra are used to obtain valuable structural and biochemical information and can also explain the status of the membrane order and dynamics [32,35–37]. Based on our knowledge, for the first time we exploited the IR-imaging spectroscopy approach in order to investigate lipid and protein alterations after inducing acute trauma in rats using the Marmarou model. Bands of the FTIR spectra are corresponding to certain biochemical components of the cellular structures such as lipid, protein, ester, nucleic acids, and carbohydrates. Detailed FTIR band assignments are defined in Table 1 [30,31].

We investigated IR absorption in the spectral range of 1500–700 cm^{-1} and 2800–3100 cm^{-1}, which are corresponding to protein and lipid components, respectively. The protein region is characteristic of amide I and amide II bands. Amide I arises from backbone C = O stretching vibrations at about 1600–1700 cm^{-1} [31,38]. The amide II arises from backbone N-H bending and C-N stretching vibrations at about 1510–1580 cm^{-1}. Amide I band is composed of many contributions assigned to β-sheet within 1635–1610 cm^{-1}, random coil at 1645–1630 cm^{-1}, and α-helical at 1660–1650 cm^{-1} (Table 1) [15,19,30]. Positions of amide I components were determined from the second-derivative intensity

Table 1
Spectral regions used for analytical interpretation for TBI study.

	Infrared band assignment	Spectral range (cm^{-1})	Comments
	Amide I	1700–1500	Total protein region
Protein components	Amide I	1700–1600	Specifically sensitive to protein secondary structure
	β-sheet	1610–1635	Functional protein, related to secondary structure of protein
	α-helix	1660–1650	Functional protein, related to secondary structure of protein
	Random coil	1645–1630	Related to secondary structure of protein
	C-H region	3100–2800	Total lipid region
Lipid component	$\nu_s CH_2$	2852–2800	to measure lipid acyl chain length
	$\nu_{as} CH_2$	2915–2930	
	$\nu_{as} CH_3$	2950–2960	to measure concentration of methyl content
	ν (C = O)	1755–1715	to measure oxidative stress
	ν (olefinic = CH)	3000–3027	to measure unsaturated lipid content

ν = stretching vibration; ν_{as} = asymmetric stretch; ν_s = symmetric stretch. *Resolutions Pro data analyzing software (V5.0), Cytospec (V2.00.03), Origin Lab (2019), Matlab (V2018b) and Cytospec (2.00.06) were used intensively to process all spectra and spectral images.

spectra, while the relative amount of the protein structures were quantified from the original absorbance spectra curve fitting [15,39]. Amide II band has multiple assignment contributions, which makes the amide I band the most important and frequent band used to explain the secondary structure of polypeptides. The shift in amide I peak, spectral alteration and the change in bandwidth indicates the protein conformation changes. Lipid region (C-H) in the spectra range of 3100–2800 cm^{-1} is characterized by bands assigned to lipid acyl ($–CH_2$) symmetric and asymmetric stretching, lipid methyl ($–CH_3$) and olefinic contents are raised at 2852 cm^{-1}, 2922 cm^{-1}, 2955 cm^{-1}, and 3012 cm^{-1}, respectively [15,30,31]. Lipid acyl chain flexibility (lipid order) is measured by using the band peak wavenumber value (peak position) of the $–CH_2$ either symmetric or antisymmetric stretching mode. If there is a shift to higher wavenumbers, it indicates that lipid order decreases (disorder) and leads to an increase in acyl chain flexibility (fluidity), if it shifts to lower wavenumber values lipid order increases e.g. acyl chain flexibility decreases [35,40].

Using the assumption that the property of individual biochemical components have their specific vibrational fingerprint, FTIR micro-spectroscopic imaging enables obtaining chemical images of the investigated tissue, where each pixel is composed of a spectrum originating from vibrational fingerprints [41]. Hematoxylin and eosin (H&E) staining of the brain section from control rat is presented in Fig. 1**A**. The three regions of interest (ROI) for this study are: a) Hippocampus, b) Corpus callosum and c) Thalamus. These regions are marked by white squares in H&E section by overlapping with FTIR images (scanned by mosaic scanning function in Agilent Cary 620 microscope) before molecular analysis.

The representative FTIR spectral normalized images of total lipid and total protein in both animal groups are shown in Fig. 1**B**. The spectral ratios images of CH_2 assym/C-H (lipid acyl chain length), CH_3 assym/C-H (methyl concertation), olefinic/C-H (unsaturated lipid content) and C-H/Amide I (total lipid/total protein) of rat brain tissues of control and 3 hrs post-TBI are shown in Fig. 1**C**. The images show that the TBI-induced changes in total lipid and total protein content were seen dramatically reduced compared to control (Fig. 1**B**). The spectral images are represented as color-coded images that are composed of a spectrum in each pixel. They are colored according to the intensity and calculated ratio values, where red color corresponds to the highest ratio, and blue color corresponds to the lowest ratio as shown in color bar.

The normalized images in Fig. 1**B** shows that the distribution of lipid and protein is homogenous in the control brain and heterogeneous in TBI animals. This indicates that biochemical and molecular alterations take place due to TBI induction. These images also show that injured animals experienced significant reduction in the lipid and protein contents, which were obvious in the white matter, cortex, hippocampus, and thalamus regions.

The spectroscopic images in Fig. 1**C** of $–CH_2$/C-H (lipid region), $–CH_3$/C-H, olefinic/C-H and lipid/protein ratios reflect the overall changes in TBI (second row) in comparison to the control (first row). The FTIR images showed that the intensity of the $–CH_2$/C-H ratio in the corpus callosum and hippocampus was reasonably higher in the control brain whereas TBI brain reflects very low intensity. This intensity in the thalamus region was moderately high in control than injured brain tissues. On the other hand, the

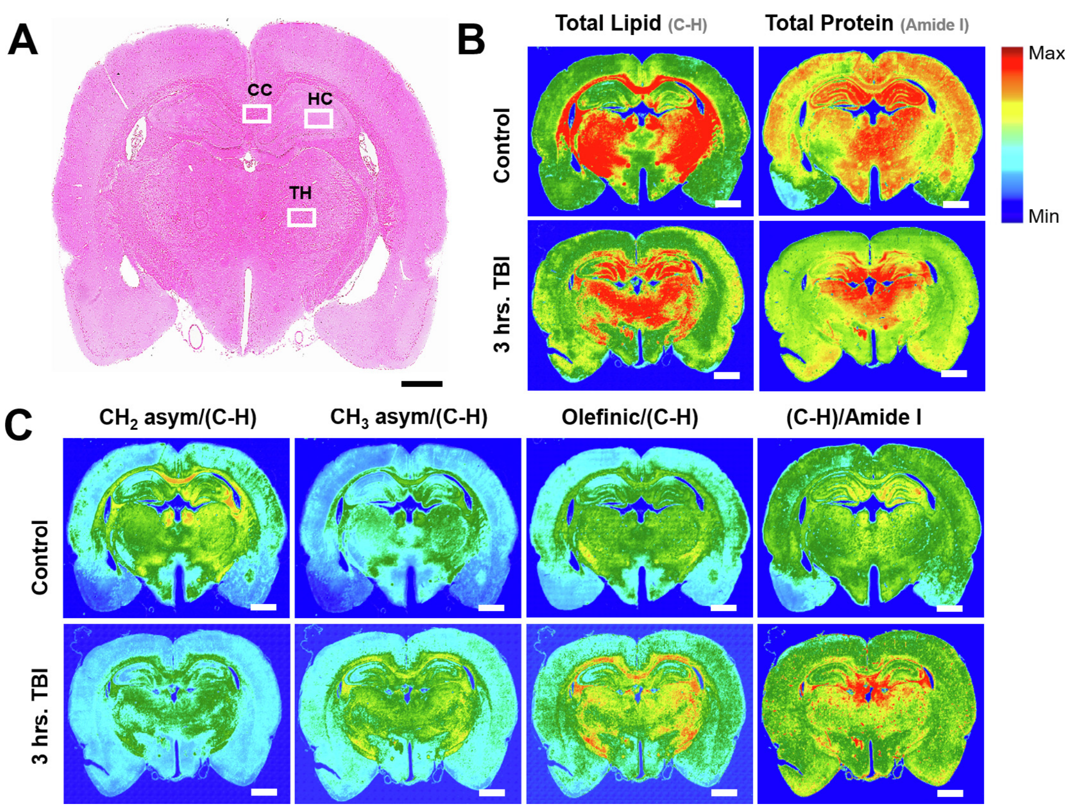

Fig. 1. Representative histological image and FTIR spectral maps of protein and lipid alterations for comparison in control (first row) and 3 h post-TBI (second row). (A) H&E image of rat brain showing regions of interests (ROI's) in white squares; HC = Hippocampus, CC = Corpus callosum and TH = Thalamus. (B) FTIR spectral maps of Total Lipid (C-H) and Total Protein (Amide I) reflecting their distribution in HC, CC and TH. (C) FTIR spectral ratio maps for CH_2 assym/C-H (lipid acyl chain length), CH_3 assym/C-H, Olefinic/C-H (unsaturated lipid content) and C-H/Amide I (Total Lipid/Total Protein). The color bar showing the intensity of the components, red = max and blue = min. Scale bar = 100 μm. (For interpretation of the references to colour in this figure legend, the reader is referred to the web version of this article.)

–CH_3/C-H intensity increased in the white matter, hippocampus and thalamus regions of TBI animals. Decreasing in the –CH_2/C-H associate with an increase –CH_3/C-H intensities indicate that TBI animals experienced fragmentation of the lipid acyl chains. The results also show that olefinic/lipid ratio (unsaturation level) increased in the TBI brains at the three regions of interest in comparison to the control group (Fig. 1**C**). The results also indicated that acute TBI affects the corpus callosum and hippocampus severely compared to thalamus region in the brain. The results suggest that although there is a diffuse effect of traumatic injury that caused reduction in lipid and protein content, this effect was consistent and resulted in total lipid/ total protein ratio to be constant compared to control animals. Subsequently, the lipid/protein ratio for different ROI's in both experimental and control groups remained almost similar.

The representative averaged and normalized FTIR spectra acquired from the ROIs, hippocampus, corpus callosum and thalamus of control and 3 h post-TBI groups in the spectral range of 4000–900 cm^{-1} are shown in Fig. 2. We focused on the protein region at 1700–1500 cm^{-1} and lipid region at 3100–2800 cm^{-1} (Fig. 2). The solid line represents the control group and the dotted lines represent TBI group. Amide I bands give information about total protein concentration and conformation [15,30,42]. The C–H stretching region that contains significant vibrations of the fatty acyl chains is a sensitive marker for the lipid content [4344]. Interestingly, the IR absorbance of the ROI regions for TBI animals has been significantly decreased comparing to the control group in both protein and lipid spectral bands.

The decrease in protein content was also supported by a significant decrease in the amide I concentration (Fig. 2). To obtain more information about changes in protein composition and structure, we calculated the band area of amide I and measured the amide I peak shift (Tables 2 and 3). The amide I spectral band area decreased in TBI compared to the control group. Since amide I band profile is corresponding to the protein biochemical structure, the change in the amide I band spectral profile of the TBI animals suggests that there are biochemical alterations in the structures of proteins. In addition, significant shifting in the wavenumber of amide I band to higher values was observed in the ROIs of TBI group in comparison to the control group that indicates alterations in protein conformation. The changes in the spectral parameters, such as the decrease in the band area and the wavenumber shifting of the amide I band (Fig. 2 and Table 2), indicate structural changes of brain tissue protein caused by TBI [45,46]. The curve deconvolution of the average IR spectrum (Fig. 2) of corpus callosum after 3 hrs post-TBI was found composed of α-helical/amide I (0.35 ± 0.0

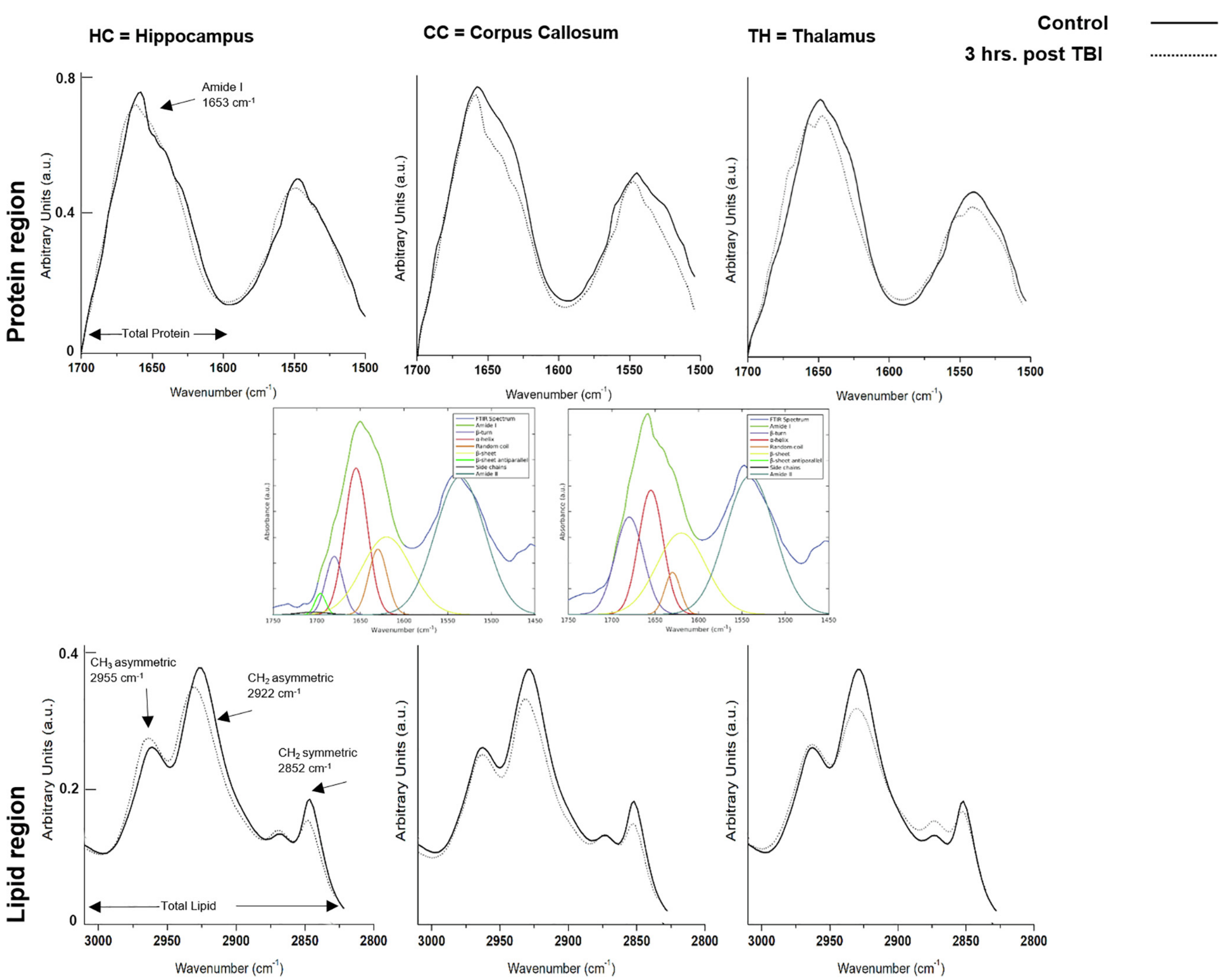

Fig. 2. Representative spectra from HC, CC and TH and their comparison. Spectral comparison in protein region (first row), representative curve fitting of corpus callosum spectra (second row) and lipid region (third row) of control and 3 h post-TBI rat brain tissues in three ROI's. The solid line represents the control and the dotted line representing TBI group.

Table 2
Protein: The band area and band position values of the amide I band in control and TBI group in the hippocampus, corpus callosum and thalamus regions.

	Control HC	Acute TBI HC	Control CC	Acute TBI CC	Control TH	Acute TBI TH
Amide I area	41.127 ± 0.023	36.954 ± 0.031**	41.311 ± 0.045	31.781 ± 0.041**	43.246 ± 0.032	35.003 ± 0.051**
Amide I position	1652.36 ± 0.45	1653.16 ± 0.33**	1652.53 ± 0.20	1653.57 ± 0.44**	1652.58 ± 0.56	1653.76 ± 0.26**

The values are the mean ± standard error of the mean for each group. The degree of significance was denoted with ** for the comparison of the control. **$p \le 0.001$.

Table 3
Ratios of protein alterations in the corpus callosum.

Region of Interest Ratios	Control - CC	Acute TBI - CC
α-helix/Amide I	53%*	35%*
β-sheet/Amide I	39%*	59%*
Random coil/Amide I	9%*	7%*

The degree of significance is denoted as * $p < 0.05$.

385), β-sheet/amide I (0.59 ± 0.0418), random coil/amide I (0.07 ± 0.0014) ($p = 0.0324$) (Table 3), which significantly changed from control CC protein secondary structure composition.

Table 4 represents the shifts in lipid component band peaks and changes in their band area that confirms the alteration in lipid order and dynamics. Lipid acyl chain flexibility (lipid order) is measured by using the wavenumber value (peak position) of the $-CH_2$ either symmetric or antisymmetric stretching mode. It is interesting to observe that there is significant shift of $\nu_s(CH_2)$, $\nu_{as}(CH_2)$ $\nu_{as}(CH_3)$ bands (which are major contributor for lipid concentration) to higher wavenumbers in the regions of interest. These results support that lipid order decreases and acyl chain flexibility increases for the 3 hrs post-TBI rat brains. In addition, the changes in the bandwidth of the C-H stretching bands reflect the alterations in the dynamics and hence fluidity of the system [47]. The increase of bandwidth and band peak shift indicates an increase in the fluidity of the system. According to the results of this study, TBI increases the membrane fluidity in the ROI's - HC, CC and TH and may lead to disordering effect in lipid-protein symmetry of the cellular structure (Fig. 2 and Table 4).

In order to determine TBI-induced alterations in the concentration and composition of biomolecules content, the band area ratios of several functional groups that belong to lipids and proteins were calculated from the ROIs for control and TBI groups. These ratios are shown in Fig. 3. Lipid and protein amounts were obtained from area of C-H region and amide I concentration, accordingly. The total lipid to total protein ratio is an important parameter in molecular membrane symmetry [48]. It was obtained by taking the ratio of the integrated areas of the C–H stretching region to the area of the amide I. Also, in order to obtain qualitative information on the lipid structure of brain tissues, olefinic band (=CH)/C-H lipid (unsaturation level), CH_2/C-H (lipid acyl chain length) and CH_3 asymmetric/C-H (methyl concentration) were calculated.

The results show that there is a significant increase in the olefinic = CH/C-H lipid ratio observed in the ROIs of 3 hrs post-TBI compared to the control group, indicating that unsaturated lipid content increased in injured brain tissues (Fig. 3). The band position and band area values of $-CH_2$ symmetric, asymmetric and $-CH_3$ asymmetric band in control and TBI group in hippocampus, corpus callosum and thalamus regions are displayed in Table 4. We observed a significant decrease in the $-CH_2$ /C-H (lipid) ratio in the ROIs of 3 hrs post-TBI group. This ratio provides information about the alterations in the acyl chains of the lipid content. The results show that there is a significant decreased in the TBI animals' group in comparison to the control group, suggesting the lipid content of TBI brains is exposed to fragmentation (acyl chain breaking down) (Figs. 1**C & **3). In addition, the methyl CH_3 asymmetric/C-H ratio increased, which also supports the results of breaking down the lipid acyl chain in the rat brain. Interestingly, in TBI animals, the total lipid/total protein ratio at the ROIs remained unchanged although a reduction in both lipid and protein contents is noted.

3. Discussion

In this study, we used high-resolution FTIR chemical imaging spectroscopy technology in order to examine the biochemical and molecular changes in rat brain tissues post-acute TBI. FTIR results indicated that white matter (corpus callosum) and hippocampus are vulnerable regions in our TBI Marmarou model. These regions are more affected after acute TBI in comparison to the thalamus region. Identifying the bio-chemical alterations at cellular and sub-cellular level of the affected brain regions is essential in trauma management as well as for developing therapeutic intervention. Membrane structure and symmetry is a very important factor for the membrane function and dynamics. This symmetry is corresponding to the lipid to protein ratio of the membrane [49,50].

The spectroscopic results revealed: (a) in the protein region, there is a reduction in the protein content; (b) the secondary structure of the protein experienced biochemical alterations; (c) in the lipid region, there is reduction in the lipid content; (d) the CH_2/lipid decreases while the CH_3/lipid indicating lipid acyl chain fragmentation and olefin/lipid is increase indicating increasing the

Table 4
Lipid: The peak position and bandwidth values of CH_2 symmetric, asymmetric and CH_3 asymmetric band in control and TBI group in the hippocampus, corpus callosum and thalamus regions.

	Control HC	Acute TBI HC	Control CC	Acute TBI CC	Control TH	Acute TBI TH
	Peak position					
$\nu_s(CH_2)$	2852.28 ± 1.023	2853.23 ± 0.068**	2853.32 ± 1.045	2854.35 ± 0.073**	2852.67 ± 1.032	2853.43 ± 1.051**
$\nu_{as}(CH_2)$	2923.45 ± 1.064	2925.18 ± 0.033**	2923.35 ± 0.20	2924.21 ± 0.041**	2923.76 ± 1.056	2924.34 ± 0.026**
$\nu_{as}(CH_3)$	2953.76 ± 0.042	2955.56 ± 0.053**	2953.36 ± 0.029	2955.54 ± 0.044**	2953.36 ± 1.034	2954.82 ± 0.023**
	Bandwidth					
$\nu_s(CH_2)$	2.34 ± 0.003	2.36 ± 0.001**	2.35 ± 0.002	2.37 ± 0.001**	2.32 ± 0.003	2.33 ± 0.002**
$\nu_{as}(CH_2)$	14.34 ± 0.013	13.35 ± 0.031**	14.35 ± 0.002	12.39 ± 0.011**	14.32 ± 0.023	13.38 ± 0.012**
$\nu_{as}(CH_3)$	5.46 ± 0.018	5.48 ± 0.011**	5.47 ± 0.021	5.49 ± 0.001**	5.46 ± 0.002	5.47 ± 0.003**

ν = stretching vibration; ν_{as} = asymmetric stretch; ν_s = symmetric stretch. The values are the mean ± standard error of the mean for each group. The degree of significance was denoted with ** for the comparison of the control. **$p \le 0.001$.

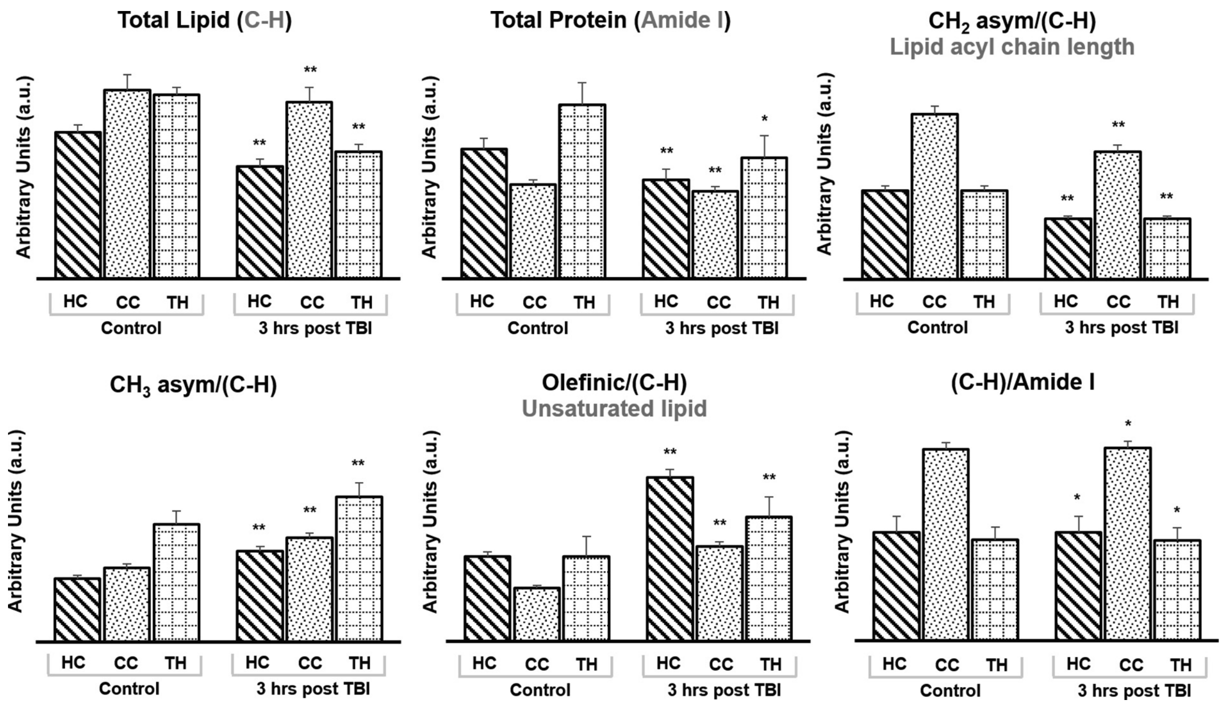

Fig. 3. Representative bar graphs for quantitative comparison of protein and lipid components. The bar graphs represent the changes in total lipid (C-H) and total protein (Amide I) (top) and changes in CH_2 assym/C-H (lipid acyl chain length), CH_3 assym/C-H, Olefinic/C-H (unsaturated lipid content) and C-H/Amide I (Total Lipid/Total Protein) ratio (bottom) for HC (wide downward diagonal bars), CC (small confetti bars) and TH (dotted grid bars) in control and 3 hrs post-TBI brain tissues. Statistical significance was determined from six animals with a MNOVA test and the 95% confidence interval. Bars represent mean ± SD. The degree of significance are denoted by * and ** where $^*p \leq 0.05$ and $^{**}p \leq 0.001$.

lipid unsaturation level in the TBI animals. Sub-cellular lipid fragmentation and changes in unsaturated lipid content could negatively affect the structure, stability, and function of the membrane [45,51] and (e) increasing in the lipid acyl chain flexibility (disordering effect in lipid) [32,35]. These results suggest that membrane fluidity was increased due to weaker interactions with neighboring hydrophobic chains. Membrane fluidity plays a major role in maintaining cell morphology and function. For instance, increased myelin fluidity promotes demyelination by decreasing myelin adhesion [52]. The membrane fluidity also determines permeability to most nonionic substances [40,45,52]. Hence, the fact that more severe demyelination and intracellular and extracellular edema occur at 3 hrs post-injury may be due to increased membrane fluidity. Instead, mild demyelination can be the result of chronic injury that may suggest that decreased membrane fluidity is a protective and repairable response. These specific alterations in biochemical components may adversely affect the neuronal and synaptic function at hippocampus, corpus callosum and thalamus as well as their performance in systematic brain function. Furthermore, the FTIR imaging and spectroscopic results revealed that although there is reduction in lipid and protein in the TBI group, the lipid/protein ratio is almost constant in both control and injured animals.

Our results are in good agreement with previous studies in regards to lipid and protein contents reduction, and protein aggregations [39,53] by FTIR spectroscopy after injury [32,39,54–56]. The amide I peak shifted to higher wavenumber representing protein structural and conformational deviations [57–59]. The total lipid and total protein content decreased significantly in the hippocampus, corpus callosum and thalamus after traumatic injury. Qualitatively shorter hydrocarbon acyl chains of lipids (less acyl - CH_2, more methyl - CH_3) and more unsaturated component of lipids - olefin = CH concentration were revealed by FTIR micro spectroscopy [54] in TBI compared to the control groups. Furthermore, the results showed that shifting of CH_2 symmetric and asymmetric of the ROIs to higher wavenumber corresponds to a decrease in the lipid order (disorder), which leads to an increase in acyl chain fluidity in injured rats [35,41,54]. The changes observed in lipid composition and concentration affecting membrane asymmetry, membrane thickness, functions of membrane and ion channel kinetics [30,48,60]. Our results also are in good agreement with the previous studies published by Caine et al. where mechanical effect and edema effect on the brain after acute ischemic stroke since they found there is a reduction in lipid and protein although the lipid/protein ratio remains constant [39].

Acute traumatic brain injury (TBI) may result in long-term consequences and degree of cognitive dysfunction is determined by the extent of damage to the brain from both the primary and secondary insults/injuries suffered. A direct physical influence to the brain or shear forces (due to rapid angular acceleration/deceleration) from the acute injury causes direct mechanical damage to neuronal and glial cells, the vasculature and strains axons. The damage from the acute injury is immediate and irreversible [61]. The regions of interest (ROIs) (hippocampus, corpus callosum and thalamus) studied in this report are extremely significant for the brain function. The hippocampus is associated more strongly to encode information and store it for longer period [62,63]. Biochemical and sub-cellular alteration in hippocampus post-acute TBI can affect memory formation and memory processing and performance [64]. Corpus callosum (CC) consists of about 200 million axons that interconnect the two hemispheres whose primary function is to integrate motor, sensory, and cognitive performances between the two brain hemispheres. In addition, corpus callosum connects cerebral, cerebellar and brain stem structures that involve in information processing. More importantly, it is predominantly comprised of a large amount of myelinated axons [15,55], containing protein-rich cytoskeleton and axoplasmic protein [53–55], whereby reduction in lipid and protein contents, associated with biochemical changes in the secondary protein structure and increased lipid fluidity due to TBI can cause slow and inefficient information processing.

The FTIR results also showed that the thalamus experience subtle effect by acute TBI. This brain region regulates consciousness, sleep, alertness, and anger. Biochemical alteration of the thalamic sub-cellular structures due to acute TBI can severely distorts the normal function of the brain. Brain neurons are well protected through blood–brain barrier, and lipid-protein structure distortion can cause serious sequence of events that affect the brain healthy environment [59]. In addition, TBI can alter membrane permeability causing concussion and neural deformation resulting in axonal swelling, and finally leads to cell death [60–62]. Biochemical alterations due to neural structural deformation caused by TBI imbalances neurotransmitters release that can affect the cellular sodium–potassium (Na^+-K^+) pump and results in distribution of membrane homeostasis [65–67].

4. Conclusions

The results of this study show that a distinct biochemical and molecular alterations in the hippocampus and corpus callosum of the brain, while this biochemical change is subtle in the thalamus. Despite the significant decrease in total lipid and total protein in the ROIs, the lipid/protein ratio in these regions remain the same. Also, increased level of protein aggregation is observed in corpus callosum. Our data also indicated that the observed molecular alterations are more consistent with mechanical and shearing effect of the tissue rather than chemical mechanism. This level of biochemical information could not be obtained with traditional bio-diagnostic methods. Therefore, the results of this study suggested that the good therapeutic approach should target the brain physical impact such as swelling and edema in order to mitigate tissue damage in the acute TBI period and administration of chemical therapy may be show benefits to manage the treatment against TBI. The results also suggested that Marmarou TBI model is a highly valuable model to study the biochemical alterations following acute TBI. Future studies, such as a time-course investigation, are now required to investigate this issue with larger number of experimental animals to determine which therapeutic strategy would translate well to the human condition.

5. Materials and methods

5.1. Experimental animals

Six male rats (11 weeks-old, Sprague-Dawley rats; Charles River Laboratories International, Wilmington, MA, United States) were used in this study. All rats were kept four per cage at room temperature under a constant 12-h light/dark cycle. A mild (by dropping weight of 450 g from 1-meter height) form of TBI is induced in two male rats (n_{TBI} = 2) and the remaining four rats served as age-matched controls ($n_{Control}$ = 4). All experimental protocols also adhered to the rules of Netherlands Council on Animal Care and approved by the prestigious University of Utrecht Animal Research Ethics Board (DEC 2013.I.08.063) prior to commencing any studies.

5.2. Procedure for TBI induction and tissue preparation

TBI is induced by a weight that freely falls from designated height through a Plexiglas tube. This weight hits a stainless-steel disc that is glued to the skull. A foam bed supports the animal's head. The steel disk prevents the skull from fracturing and distributes the impact power over a larger brain area. A falling height of 1 m, using a weight of 450 g induces mild TBI. Brains are extracted, kept in −80 °C until tissue preparation, fixed in 4% paraformaldehyde (PFA) for 24 h and embedded in paraffin 3 hrs after TBI induction. The paraffin blocks were kept upside down on cold plate before slicing for Hematoxylin and Eosin (H&E) staining and FTIR studies. Paraffin embedded tissue blocks were serially cut into slices of 10 μm thickness using Leica RM 2155 semi-automated rotary microtome (Germany) at bregma −3.30 mm. The regions of interest (ROI) for this study were: (a) Hippocampus, (b) Corpus callosum and (c) Thalamus. Ten serial and consecutive 10 μm sections from each rat were obtained for FTIR analysis and histology staining analysis.

5.3. FTIR data acquisition and pre-processing

The brain sections for FTIR analysis for TBI animal model was mounted on MirrIR low-e microscope slides (Kevley Technologies, 8696 Ranch Dr, Chesterland, Ohio, USA), deparaffinized, dried and stored in a desiccator at room temperature. FTIR spectra were recorded using an Agilent FTIR Cary 620 micro-spectrometer in reflection mode within the range of 4000–700 cm^{-1} with 64 scans per spectrum, 4 cm^{-1} spectral resolution and spatial resolution 80 μm. FTIR chemical images were recorded using a 64 × 64 Mercury Cadmium Telluride (MCT) Focal Plane Array (FPA) liquid nitrogen cooled detector in mosaic mode. FTIR imaging was performed with a pixel size of 5.5 × 5.5 μm. Resolution Pro. Software (version 5.0), Cytospec (version 2.00.06) and OriginPro (2019) were used for image generation and pre-processing of all spectral data. Spectra were acquired away from the border between tissue regions and the substrate to avoid resonance Mie scattering. Detailed FTIR data acquisition and pre-processing of the data are explained in our previous work [15–17]. From the corpus callosum and thalamus, approximately 50–70 spectra were collected and averaged from both control and TBI group and then compared in this study. For the hippocampus, as it is a more heterogeneous region, the area was divided into 10 minor regions, approximately 10–15 spectra from each minor region were collected. All these ~ 100–150 spectra were averaged for homogenous comparison.

5.4. Statistical analysis

Statistical analysis was performed using R (v3.6). After testing data for normal distribution and homogeneity of variance, a one-way multivariate analysis of variance (MANOVA) was carried out on the five measurements using a Wilks test. The coefficient of variation was calculated for each parameter in each animal and the data summarized as the mean and standard deviations for each group. The (two-tailed) $p \le 0.05$ were considered as statistically significant for multiple comparisons ($^*p \le 0.05$; $^{**}p \le 0.001$) with a 95% confidence interval.

CRediT authorship contribution statement

Fazle Rakib: Conceptualization, Methodology, Resources, Writing - original draft, Writing - review & editing. **Khalid Al-Saad:** Conceptualization, Methodology, Resources, Writing - original draft, Writing - review & editing. **Tariq Ahmed:** Conceptualization, Methodology, Resources, Writing - original draft, Writing - review & editing. **Ehsan Ullah:** Conceptualization, Methodology, Resources, Writing - original draft, Writing - review & editing. **George E. Barreto:** Methodology, Resources, Writing - original draft, Writing - review & editing. **Ghulam Md Ashraf:** Methodology, Resources, Writing - original draft, Writing - review & editing. **Mohamed H.M. Ali:** Conceptualization, Methodology, Resources, Writing - original draft, Writing - review & editing, Supervision.

Declaration of Competing Interest

None.

Acknowledgements

The authors would like to thank Drs. Geralda van Tilborg, Rick M. Dijkhuizen (Biomedical MR Imaging and Spectroscopy Group, Center for Image Sciences, University Medical Center Utrecht, Utrecht, Netherlands) for providing us the brain samples for this study. The authors also like to thank Mr. Xyrus and Mrs. Ann from Al Ahli Hospital for the great effort in preparing tissues samples for our analysis.

Funding

"This study was made possible by a NPRP Award [7-1648-3-420-4] from the Qatar National Research Fund (a member of The Qatar Foundation). The statements made herein are solely the responsibility of the authors."

References

[1] G.A. Zitnay, Lessons from national and international TBI societies and funds like NBIRTT, Acta Neurochir. Suppl. (2005), https://doi.org/10.1007/3-211-27577-0_22.
[2] Y. Xiong, A. Mahmood, M. Chopp, Animal models of traumatic brain injury, Nat. Rev. Neurosci. 14 (2013) 128–142, https://doi.org/10.1038/nrn3407.
[3] H. Sierra, M. Cordova, C.-S.-J. Chen, M. Rajadhyaksha, Confocal Imaging-Guided Laser Ablation of Basal Cell Carcinomas: An Ex Vivo Study, J. Invest. Dermatol. 135 (2015) 612–615, https://doi.org/10.1038/jid.2014.371.
[4] E.D. Bigler, Anterior and Middle Cranial Fossa in Traumatic Brain Injury: Relevant Neuroanatomy and Neuropathology in the Study of Neuropsychological Outcome, Neuropsychology. (2007), https://doi.org/10.1037/0894-4105.21.5.515.
[5] T.W. Mcallister, M.B. Stein, Effects of psychological and biomechanical trauma on brain and behavior, Ann. N. Y. Acad. Sci. (2010), https://doi.org/10.1111/j.1749-6632.2010.05720.x.
[6] V.E. Johnson, W. Stewart, D.H. Smith, Axonal pathology in traumatic brain injury, Exp. Neurol. (2013), https://doi.org/10.1016/j.expneurol.2012.01.013.
[7] T.M. Reeves, L.L. Phillips, J.T. Povlishock, Myelinated and unmyelinated axons of the corpus callosum differ in vulnerability and functional recovery following traumatic brain injury, Exp. Neurol. (2005), https://doi.org/10.1016/j.expneurol.2005.07.014.
[8] D.B. Arciniegas, Addressing neuropsychiatric disturbances during rehabilitation after traumatic brain injury: Current and future methods, Dialogues Clin. Neurosci., 2011.
[9] K.D. Statler, K.L. Janesko, J.A. Melick, R.S.B. Clark, L.W. Jenkins, P.M. Kochanek, Hyperglycolysis is exacerbated after traumatic brain injury with fentanyl vs. isoflurane anesthesia in rats, Brain Res. (2003), https://doi.org/10.1016/j.brainres.2003.09.042.
[10] A.L. Lin, E.K. Avila, Neurologic Emergencies in the Patients With Cancer, J. Intensive Care Med. 32 (2017) 99–115, https://doi.org/10.1177/0885066615619582.
[11] W.B. Barr, Mild traumatic brain injury, in: Handb. Neuropsychol. Trauma. Brain Inj., 2014. doi:10.1007/978-1-4939-0784-7_18.
[12] E.M. Umile, M.E. Sandel, A. Alavi, C.M. Terry, R.C. Plotkin, Dynamic imaging in mild traumatic brain injury: Support for the theory of medial temporal vulnerability, Arch. Phys. Med. Rehabil. (2002), https://doi.org/10.1053/apmr.2002.35092.
[13] K.E. Wartenberg, S.A. Mayer, Intracerebral hemorrhage, in: Stroke Book, Second Ed., 2013. doi:10.1017/CBO9781139344296.014.
[14] M.J. Hackett, C.J. Britz, P.G. Paterson, H. Nichol, I.J. Pickering, G.N. George, In situ biospectroscopic investigation of rapid ischemic and postmortem induced biochemical alterations in the rat brain, ACS Chem. Neurosci. (2015), https://doi.org/10.1021/cn500157j.
[15] M.H.M. Ali, F. Rakib, E.M. Abdelalim, A. Limbeck, R. Mall, E. Ullah, N. Mesaeli, D. McNaughton, T. Ahmed, K. Al-Saad, Fourier-Transform Infrared Imaging Spectroscopy and Laser Ablation -ICPMS New Vistas for Biochemical Analyses of Ischemic Stroke in Rat Brain, Front. Neurosci. 12 (2018), https://doi.org/10.3389/fnins.2018.00647.
[16] M.H.M. Ali, F. Rakib, K. Al-Saad, R. Al-Saady, E. Goormaghtigh, An Innovative Platform Merging Elemental Analysis and Ftir Imaging for Breast Tissue Analysis, Sci. Rep. 9 (2019) 9854, https://doi.org/10.1038/s41598-019-46056-4.
[17] M.H.M. Ali, F. Rakib, V. Nischwitz, E. Ullah, R. Mall, A. Shraim, M. Ahmad, Z. Ghouri, D. McNaughton, S. Küppers, T. Ahmed, K. Al-Saad, Application of FTIR and LA-ICPMS Spectroscopies as a Possible Approach for Biochemical Analyses of Different Rat Brain Regions, Appl. Sci. 8 (2018) 2436, https://doi.org/10.3390/app8122436.
[18] S. Caine, P. Heraud, M.J. Tobin, D. McNaughton, C.C.A. Bernard, The application of Fourier transform infrared microspectroscopy for the study of diseased central nervous system tissue, Neuroimage. (2012), https://doi.org/10.1016/j.neuroimage.2011.11.033.
[19] M.H.M. Ali, S.M. Toor, F. Rakib, R. Mall, E. Ullah, K. Mroue, P.R. Kolatkar, K. Al-saad, E. Elkord, Investigation of the E ff ect of PD-L1 Blockade on Triple Negative Breast Cancer Cells Using Fourier Transform Infrared Spectroscopy, 2 (n.d.) 1–16.
[20] M.H. Ali, F. Rakib, K. Al-Saad, R. Al-Saady, F.M. Lyng, E. Goormaghtigh, A simple model for cell type recognition using 2D-correlation analysis of FTIR images from breast cancer tissue, J. Mol. Struct. (2018), https://doi.org/10.1016/j.molstruc.2018.03.044.
[21] A. Balbekova, M. Bonta, S. Török, J. Ofner, B. Döme, A. Limbeck, B. Lendl, FTIR-spectroscopic and LA-ICP-MS imaging for combined hyperspectral image analysis of tumor models, Anal. Methods. (2017), https://doi.org/10.1039/c7ay01369h.
[22] S.S.J. Ahmed, W. Santosh, S. Kumar, T.H. Thanka Christlet, Neural network algorithm for the early detection of Parkinson's disease from blood plasma by FTIR micro-spectroscopy, Vib. Spectrosc. (2010), https://doi.org/10.1016/j.vibspec.2010.01.019.
[23] L.M. Miller, M.W. Bourassa, R.J. Smith, FTIR spectroscopic imaging of protein aggregation in living cells, Biochim. Biophys. Acta - Biomembr. (2013), https://doi.org/10.1016/j.bbamem.2013.01.014.
[24] L.M. Miller, M.W. Bourassa, R.J. Smith, Biochimica et Biophysica Acta FTIR spectroscopic imaging of protein aggregation in living cells ☆, BBA - Biomembr. (2013), https://doi.org/10.1016/j.bbamem.2013.01.014.
[25] D. Yonar, L. Ocek, B.I. Tiftikcioglu, Y. Zorlu, F. Severcan, Relapsing-Remitting Multiple Sclerosis diagnosis from cerebrospinal fluids via Fourier transform infrared spectroscopy coupled with multivariate analysis, Sci. Rep. (2018), https://doi.org/10.1038/s41598-018-19303-3.
[26] A. Sevinc, D. Yonar, F. Severcan, Investigation of neurodegenerative diseases from body fluid samples using Fourier transform infrared spectroscopy, Biomed. Spectrosc. Imaging. (2015), https://doi.org/10.3233/bsi-150123.
[27] R.J. Tidy, V. Lam, N. Fimognari, J.C. Mamo, M.J. Hackett, FTIR studies of the similarities between pathology induced protein aggregation in vivo and chemically induced protein aggregation ex vivo, Vib. Spectrosc. (2017), https://doi.org/10.1016/j.vibspec.2016.09.016.
[28] K.L. Summers, N. Fimognari, A. Hollings, M. Kiernan, V. Lam, R.J. Tidy, D. Paterson, M.J. Tobin, R. Takechi, G.N. George, I.J. Pickering, J.C. Mamo, H.H. Harris, M.J. Hackett, A Multimodal Spectroscopic Imaging Method to Characterize the Metal and Macromolecular Content of Proteinaceous Aggregates ("Amyloid Plaques"), Biochemistry. (2017), https://doi.org/10.1021/acs.biochem.7b00262.
[29] A.D. Surowka, M. Pilling, A. Henderson, H. Boutin, L. Christie, M. Szczerbowska-Boruchowska, P. Gardner, FTIR imaging of the molecular burden around Aβ deposits in an early-stage 3-Tg-APP-PSP1-TAU mouse model of Alzheimer's disease, Analyst. (2017), https://doi.org/10.1039/c6an01797e.
[30] G. Cakmak, L.M. Miller, F. Zorlu, F. Severcan, Amifostine, a radioprotectant agent, protects rat brain tissue lipids against ionizing radiation induced damage: An FTIR microspectroscopic imaging study, Arch. Biochem. Biophys. 520 (2012) 67–73, https://doi.org/10.1016/j.abb.2012.02.012.
[31] M.H.M. Ali, F. Rakib, V. Nischwitz, E. Ullah, R. Mall, A. Shraim, M. Ahmad, Z. Ghouri, D. McNaughton, S. Küppers, T. Ahmed, K. Al-Saad, Application of FTIR and LA-ICPMS Spectroscopies as a Possible Approach for Biochemical Analyses of Different Rat Brain Regions, Appl. Sci. (2018), https://doi.org/10.3390/app8122436.
[32] G. Cakmak, I. Togan, F. Severcan, 17β-Estradiol induced compositional, structural and functional changes in rainbow trout liver, revealed by FT-IR spectroscopy: A comparative study with nonylphenol, Aquat. Toxicol. 77 (2006) 53–63, https://doi.org/10.1016/j.aquatox.2005.10.015.
[33] F. Severcan, G. Gorgulu, S.T. Gorgulu, T. Guray, Rapid monitoring of diabetes-induced lipid peroxidation by Fourier transform infrared spectroscopy: Evidence from rat liver microsomal membranes, Anal. Biochem. (2005), https://doi.org/10.1016/j.ab.2005.01.011.
[34] F. Severcan, P.I. Haris, Fourier transform infrared spectroscopy suggests unfolding of loop structures precedes complete unfolding of pig citrate synthase, Biopolymers. (2003), https://doi.org/10.1002/bip.10392.
[35] F. Severcan, Vitamin e decreases the order of the phospholipid model membranes in the gel phase: An FTIR study, Biosci. Rep. (1997), https://doi.org/10.1023/A:1027341731230.
[36] H. Takahashi, S.W. French, P.T.T. Wong, Alterations in Hepatic Lipids and Proteins by Chronic Ethanol Intake: A High-Pressure Fourier Transform Infrared Spectroscopic Study on Alcoholic Liver Disease in the Rat, Alcohol. Clin. Exp. Res. (1991), https://doi.org/10.1111/j.1530-0277.1991.tb01859.x.
[37] F. Severcan, I. Sahin, N. Kazanci, Melatonin strongly interacts with zwitterionic model membranes-evidence from Fourier transform infrared spectroscopy and differential scanning calorimetry, Biochim. Biophys. Acta - Biomembr. (2005), https://doi.org/10.1016/j.bbamem.2004.12.009.
[38] C. Petibois, B. Desbat, Clinical application of FTIR imaging: New reasons for hope, Trends Biotechnol. (2010), https://doi.org/10.1016/j.tibtech.2010.07.003.
[39] S. Caine, M.J. Hackett, H. Hou, S. Kumar, J. Maley, Z. Ivanishvili, B. Suen, A. Szmigielski, Z. Jiang, N.J. Sylvain, H. Nichol, M.E. Kelly, A novel multi-modal platform to image molecular and elemental alterations in ischemic stroke, Neurobiol. Dis. (2016), https://doi.org/10.1016/j.nbd.2016.03.006.

[40] S. Ergun, P. Demir, T. Uzbay, F. Severcan, Agomelatine strongly interacts with zwitterionic DPPC and charged DPPG membranes, Biochim. Biophys. Acta - Biomembr. (2014), https://doi.org/10.1016/j.bbamem.2014.07.025.

[41] F. Kucuk Baloglu, S. Garip, S. Heise, G. Brockmann, F. Severcan, FTIR imaging of structural changes in visceral and subcutaneous adiposity and brown to white adipocyte transdifferentiation, Analyst. 140 (2015) 2205–2214, https://doi.org/10.1039/C4AN02008A.

[42] K.P. Ishida, P.R. Griffiths, Comparison of the amide I/II intensity ratio of solution and solid-state proteins sampled by transmission, attenuated total reflectance, and diffuse reflectance spectrometry, Appl. Spectrosc. 47 (1993) 584–589, https://doi.org/10.1366/0003702934067306.

[43] J. Kneipp, P. Lasch, E. Baldauf, M. Beekes, D. Naumann, Detection of pathological molecular alterations in scrapie-infected hamster brain by Fourier transform infrared (FT-IR) spectroscopy, Biochim. Biophys. Acta - Mol. Basis Dis. (2000), https://doi.org/10.1016/S0925-4439(00)00021-1.

[44] O. Bozkurt, M. Severcan, F. Severcan, Diabetes induces compositional, structural and functional alterations on rat skeletal soleus muscle revealed by FTIR spectroscopy: A comparative study with EDL muscle, in, Analyst (2010), https://doi.org/10.1039/c0an00542h.

[45] F. Kucuk Baloglu, S. Garip, S. Heise, G. Brockmann, F. Severcan, FTIR imaging of structural changes in visceral and subcutaneous adiposity and brown to white adipocyte transdifferentiation, Analyst. (2015), https://doi.org/10.1039/c4an02008a.

[46] K.B. F., B. G., S. F., Biophysical characterization and diagnosis of obesity from adipose tissue by fourier transform infrared (FTIR) spectroscopy and imaging, Obes. Facts. (2018). doi:10.1159/000489691 LK - http://sfx.library.uu.nl/utrecht?sid=EMBASE&issn=16624033&id=doi:10.1159%2F000489691&atitle=Biophysical+characterization+and+diagnosis+of+obesity+from+adipose+tissue+by+fourier+transform+infrared+%28FTIR%29+spectroscopy+and+imaging&stitle=Obes.+Facts&title=Obesity+Facts&volume=11&issue=&spage=40&epage=&aulast=Kucuk+Baloglu&aufirst=F.&auinit=F.&aufull=Kucuk+Baloglu+F.&coden=&isbn=&pages=40-&date=2018&auinit1=F&auinitm=.

[47] S. Turker, S. Wassall, W. Stillwell, F. Severcan, Convulsant agent pentylenetetrazol does not alter the structural and dynamical properties of dipalmitoylphosphatidylcholine model membranes, J. Pharm. Biomed. Anal. (2011), https://doi.org/10.1016/j.jpba.2010.09.002.

[48] N. Simsek Ozek, S. Tuna, A.E. Erson-Bensan, F. Severcan, Characterization of microRNA-125b expression in MCF7 breast cancer cells by ATR-FTIR spectroscopy, Analyst (2010), https://doi.org/10.1039/c0an00543f.

[49] B. Szalontai, Y. Nishiyama, Z. Gombos, N. Murata, Membrane dynamics as seen by Fourier transform infrared spectroscopy in a cyanobacterium, Synechocystis PCC 6803 - The effects of lipid unsaturation and the protein-to-lipid ratio, Biochim. Biophys. Acta - Biomembr. (2000), https://doi.org/10.1016/S0005-2736(00)00323-0.

[50] N. Toyran, F. Zorlu, G. Dönmez, K. Öğe, F. Severcan, Chronic hypoperfusion alters the content and structure of proteins and lipids of rat brain homogenates: A Fourier transform infrared spectroscopy study, Eur. Biophys. J. (2004), https://doi.org/10.1007/s00249-004-0396-1.

[51] A.W. Smith, Lipid-protein interactions in biological membranes: A dynamic perspective, Biochim. Biophys. Acta - Biomembr. (2012), https://doi.org/10.1016/j.bbamem.2011.06.015.

[52] J. Zhang, L. Liu, J. Mu, T. Yang, N. Zheng, H. Dong, Chemical Analysis in the Corpus Callosum Following Traumatic Axonal Injury using Fourier Transform Infrared Microspectroscopy: A Pilot Study, J. Forensic Sci. 60 (2015) 1488–1494, https://doi.org/10.1111/1556-4029.12871.

[53] M.J. Hackett, M. Desouza, S. Caine, B. Bewer, H. Nichol, P.G. Paterson, F. Colbourne, A new method to image heme-Fe, total Fe, and aggregated protein levels after intracerebral hemorrhage, ACS Chem. Neurosci. (2015), https://doi.org/10.1021/acschemneuro.5b00037.

[54] J. Zhang, L. Liu, J. Mu, T. Yang, N. Zheng, H. Dong, Chemical Analysis in the Corpus Callosum Following Traumatic Axonal Injury using Fourier Transform Infrared Microspectroscopy: A Pilot Study, J. Forensic Sci. (2015), https://doi.org/10.1111/1556-4029.12871.

[55] R. Gasper, J. Dewelle, R. Kiss, T. Mijatovic, E. Goormaghtigh, IR spectroscopy as a new tool for evidencing antitumor drug signatures, Biochim. Biophys. Acta - Biomembr. (2009), https://doi.org/10.1016/j.bbamem.2009.02.016.

[56] M. Shinitzky, P. Henkart, Fluidity of Cell Membranes—Current Concepts and Trends, Int. Rev. Cytol. (1979), https://doi.org/10.1016/S0074-7696(08)61261-9.

[57] J. Zhang, F. Niu, H. Dong, L. Liu, J. Li, S. Li, Characterization of Protein Alterations in Damaged Axons in the Brainstem Following Traumatic Brain Injury Using Fourier Transform Infrared Microspectroscopy: A Preliminary Study, J. Forensic Sci. (2015), https://doi.org/10.1111/1556-4029.12743.

[58] J. Zhang, P. Huang, Z. Wang, H. Dong, Application of FTIR spectroscopy for traumatic axonal injury: a possible tool for estimating injury interval, Biosci. Rep. (2017), https://doi.org/10.1042/bsr20170720.

[59] P.I. Haris, F. Severcan, FTIR spectroscopic characterization of protein structure in aqueous and non-aqueous media, in, J. Mol. Catal. - B Enzym. (1999), https://doi.org/10.1016/S1381-1177(99)00030-2.

[60] F. Korkmaz, F. Severcan, Effect of progesterone on DPPC membrane: Evidence for lateral phase separation and inverse action in lipid dynamics, Arch. Biochem. Biophys. (2005), https://doi.org/10.1016/j.abb.2005.06.013.

[61] K.R. Walker, G. Tesco, Molecular mechanisms of cognitive dysfunction following traumatic brain injury, Front. Aging Neurosci. (2013), https://doi.org/10.3389/fnagi.2013.00029.

[62] E.T. Rolls, A theory of hippocampal function in memory, Hippocampus. (1996), https://doi.org/10.1002/(SICI)1098-1063(1996)6:6<601::AID-HIPO5>3.0.CO;2-J.

[63] P. Andersen, R. Morris, D. Amaral, T. Bliss, J. O' Keefe, The Hippocampus Book, 2009. doi:10.1093/acprof:oso/9780195100273.001.0001.

[64] M.J.A.G. Henckens, E.J. Hermans, Z. Pu, M. Joëls, G. Fernández, Stressed memories: How acute stress affects memory formation in humans, J. Neurosci. (2009), https://doi.org/10.1523/JNEUROSCI.1184-09.2009.

[65] C.C. Giza, D.A. Hovda, The new neurometabolic cascade of concussion, Neurosurgery. (2014), https://doi.org/10.1227/NEU.0000000000000505.

[66] D.A. Hovda, C.C. Giza, M. Bergsneider, P.M. Vespa, Concussions in Athletics, Springer, New York, New York NY (2014), https://doi.org/10.1007/978-1-4939-0295-8.

[67] A.C. Mckee, D.H. Daneshvar, The neuropathology of traumatic brain injury, Handb. Clin. Neurol. (2015), https://doi.org/10.1016/B978-0-444-52892-6.00004-0.